International Journal of Biological Macromolecules 47 (2010) 661–667

Contents lists available at ScienceDirect

International Journal of Biological Macromolecules

journal homepage: www.elsevier.com/locate/ijbiomac

Imaging recognition events between human IgG and rat anti-human IgG by atomic force microscopy

Zhengjian Lv, Jianhua Wang*, Guoping Chen, Linhong Deng

Key Laboratory of Biorheological Science and Technology, Ministry of Education, and Institute of Biochemistry and Biophysics, College of Bioengineering, Chongqing University, No. 174, Shazhengjie, Shapingba District, Chongqing 400044, China

ARTICLE INFO

Article history:
Received 17 June 2010
Received in revised form 23 August 2010
Accepted 23 August 2010
Available online 9 September 2010

Keywords:
Rat anti-human IgG
Human IgG
Self-assembled monolayer
Atomic force microscopy
Phase imaging

ABSTRACT

Chemically immobilized rat anti-human immunoglobulin (IgG) monolayers on thiols modified gold substrates were fabricated using self-assembled monolayer (SAM) method. The antibody monolayers were imaged before and after free human IgG treated, whilst recognition events between antigen and antibody were monitored by contact mode atomic force microscopy (CM-AFM) and tapping mode AFM (TM-AFM), with topographic and/or phase images being recorded. The obtained images with different surface compositions show distinct nanostructures, indicating occurrence of recognition and binding events of antigen–antibody. The size of the observed surface structures of the antibody monolayer, when tip broaden effect had been taken into account, was very close to the actual size of the antibody molecule. Thus, these results suggest CM-AFM is capable of, and proven satisfactory in detecting protein–protein interactions (PPIs), providing the sample was prepared appropriately and the scanning parameters were set adequately. Moreover, phase imaging can serve as a real time contrast enhancement technique to TM-AFM in terms of highlighting edges and clearly observing fine features.

1. Introduction

Antibody based protein–protein interactions (PPIs) play crucial roles in biosensors [1,2], molecular recognition at single-molecule scale [3,4], and medical diagnostics [5,6]. So far, a number of methods have been developed for PPIs studies, including surface force apparatus (SFA) [7], surface plasmon resonance (SPR) [8], radioimmunoassay (RIA) [9], enzyme immunoassay (EIA) [10], and atomic force microscopy (AFM) [11]. Compared to other methods, AFM is advantageous in terms of high spatial resolution, allowing measurements in near physiological environment and free of special sample preparation [12]. Hence, AFM opens new avenues to study pathways of PPIs. AFM is now an established technique to investigate the physical behaviors of PPIs, such as adhesive force, friction force and energy dissipation [13–16]. Moreover, along with the ability to image the topographies of protein molecules with nanoscale resolution and down to single molecular level, AFM can be served as a powerful tool to monitor the specific interaction (recognition) between antigen and antibody. As for topographical studies, contact mode AFM (CM-AFM) was employed to obtain high-resolution images, whereas the tapping mode atomic force microscopy (TM-AFM) was often used to prevent the deformation of samples because it substantially reduces the lateral force [17].

Upon CM-AFM, it is noteworthy that the AFM tip will introduce broaden effect as illustrated in Fig. 1. A round shape for tip is assumed as revealed by electron micrographs. A half sphere structure is assumed as a protein molecule immobilized on thiol modified gold substrate. When the tip scans over the surface, it constantly contacts with the protein layer: as the tip approaches an elevation from the side of the protein contour, it will detect the elevation with its outer edge before the centre of the tip reaches the point where the elevation starts [18], such effect introduced in the CM-AFM is called broaden effect.

$$x^2 + R^2 = (r + R)^2 \quad (1)$$

$$x = \sqrt{2Rr + r^2} \quad (2)$$

$$D = 2x = 2\sqrt{2Rr + r^2} \quad (3)$$

where R is the tip radii, r is the real width of protein molecule, x and D are the apparent widths of protein molecule, respectively. The observed image of the protein is illustrated in the upper-right corner of Fig. 1.

In recent years, based on the TM-AFM, a novel extension imaging mode termed phase imaging has been explored, in which case, the phase lag of the cantilever oscillation relative to the drive signal, accompanied with topography data, is monitored. Phase imaging not only highlights edges to obtain better contrast and clearer

* Corresponding author. Tel.: +86 23 65102507; fax: +86 23 65102507.
E-mail addresses: wjh@cqu.edu.cn, cqubio@hotmail.com (J. Wang).

0141-8130/$ – see front matter © 2010 Elsevier B.V. All rights reserved.
doi:10.1016/j.ijbiomac.2010.08.017

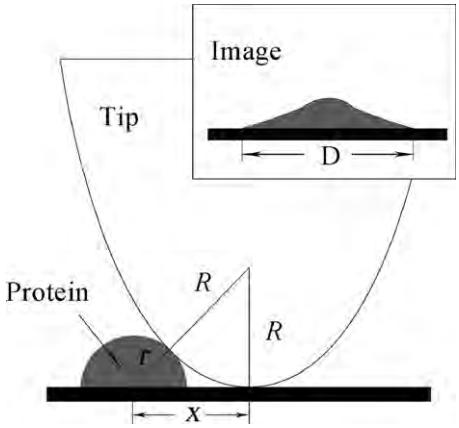

Fig. 1. The broaden effect of AFM tip. In which, *R* is the tip radii, *r* is the real width of sample structure, *x* and *D* are the apparent widths of sample structure, respectively. When the CM-AFM operates, as the tip approaches an elevation from the side, it will detect the elevation with its outer edge before the centre of the tip has reached the point where the elevation starts, as a result, the fine structure will be enlarged. The final observed image is shown in the upper-right corner.

observation of protein molecules compared to conventional AFM imaging, but also provides information of surface properties of the molecules [19,20]. Consequently, phase imaging is emerging as a powerful tool for mapping variations in sample properties with superior details and with no cost in speed or resolution.

One of the major challenges, however, for AFM imaging is the sample preparation, in particular, the coating of protein molecules onto the surface of the gold substrates, and the AFM tips (functionalizing AFM tip or tip chemistry). Currently, a couple of excellent methods have been used to immobilize protein molecules, including self-assembled monolayer (SAM), silanization method, and 3-aminopropyltriethoxysilane (APTES) method [21,22]. SAM method has been developed over two decades and extensively used by biochemists.

Until now, AFM has been successfully applied for revealing the recognition events between antigen and antibody, such as histone H3/polyclonal anti-histone H3 antibody [23], insulin/scFv antibody [24]. However, the lack of comparison between different imaging modes under controlled conditions raised a question about how phase imaging is helpful to topographic imaging and whether CM-AFM is reliable and reproducible for imaging biological events. The motivation of this work was to try addressing such issues.

2. Materials and methods

2.1. Mechanism of SAM

The mechanism of SAM method is simple [22]: sulfur containing molecules (thiols, sulfides and disulfides) have a strong affinity for gold, yielding an Au–S bond. The reaction is spontaneous, and thiol-based SAM is obtained by simple immersion of the gold substrate into a solution of the selected thiol. The SAM will be ideally composed of tightly packed and well-ordered chains. SAM with carboxyl tail groups can be activated by two chemicals: 1-ethyl-3-(dimethylaminopropyl) carbodiimide hydrochloride (EDC) and N-hydroxysulfosuccinimide (NHS) to form an active ester, the activated SAM was then soaked into protein solution for 24 h to form protein monolayer. The mechanism of protein immobilized on the thiols modified gold surface is depicted in Fig. 2.

2.2. Preparation of gold substrates

Gold substrates were prepared by vapor deposition of gold onto freshly cleaved mica in a high vacuum evaporator at $\sim 10^{-7}$ Torr. Mica substrates were preheated to 325 °C for 2 h by a radiator heater before deposition. Evaporation rates were 0.1–0.3 nm/s, and the final thickness of gold films was ~200 nm. A chromium layer was also vapor deposited and sandwiched between the gold and mica to strengthen the adhesion between the surfaces. The gold-coated substrate was then annealed in H_2 flame for 1 min before use.

2.3. Formation of MHA film

The bare gold substrates were soaked into a hot piranha solution (v/v H_2SO_4:H_2O_2 = 3:1) for 30 min to clean the surface. The cleaning process was carried out with extreme care because piranha solution is highly reactive and may explode when in contact with organic solvents. Then SAM was formed by immersing the bare gold substrate in 1 mM 16-mercaptohexadecanoic acid in ethanol solution for 24 h. The formed SAM was supersonicated in pure ethanol for 2 min to remove unbound thiol molecules, then rinsed sequentially with pure ethanol, ultra pure water, and finally air-dried in a N_2 stream.

2.4. Protein immobilization onto the MHA-modified gold substrate

Protein immobilization to SAM was carried out as described before [25]. In brief, SAM with carboxylic acid terminal groups were activated by 2 mg/mL NHS and 2 mg/mL EDC in phosphate buffered saline solution for 1 h, and subsequently rinsed thoroughly with ultra pure water, and air-dried in N_2 stream. The activated SAM was then immersed into 10 μg/mL rat anti-human IgG in PBS solution at 4 °C for 12 h. Finally, the prepared specimens of SAM with immobilized protein were stored in PBS solution at 4 °C before use.

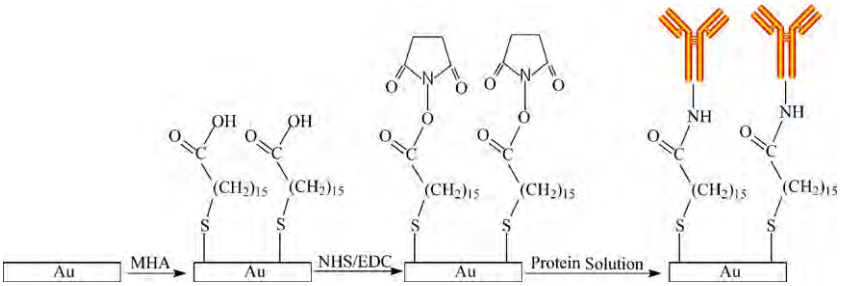

Fig. 2. A schematic illustration of the SAM method used in this study. From left to right, the bare gold substrate was firstly modified by soaking it into the ethanol solution of 16-mercaptohexadecanoic acid (MHA) for 24 h, the reaction system spontaneously yielded an Au–S bond, resulting formation of a MHA film on gold substrate. The MHA film was immersed into protein (rat anti-human IgG) solution after it was activated by NHS and EDC. The temperature of reaction was controlled at 4 °C and incubated for 8 h. Finally, a well-defined protein monolayer on the MHA-modified gold substrate was successfully fabricated.

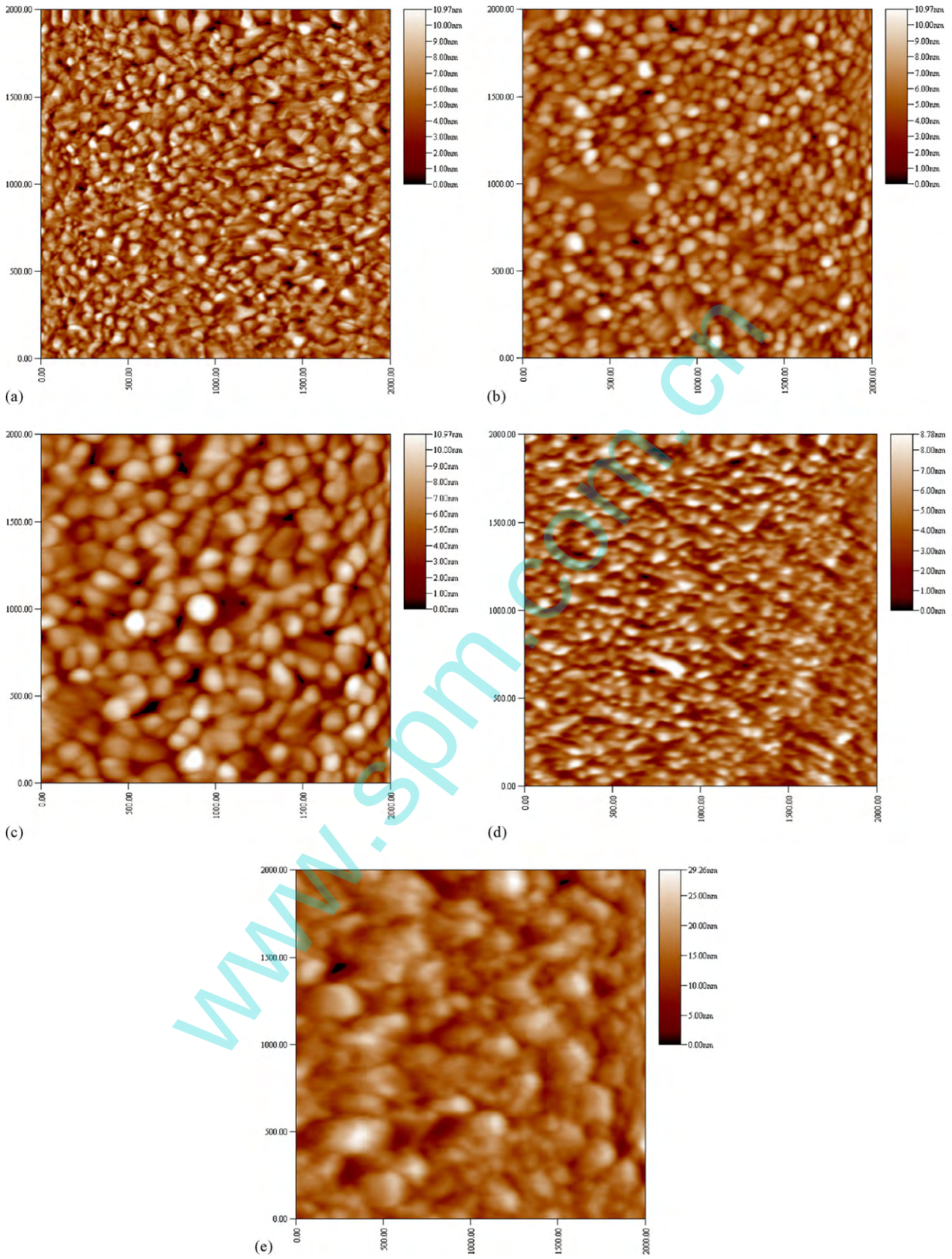

Fig. 3. Topographic images of the bare gold (a), the rat anti-human IgG monolayer (b), the human IgG/rat anti-human IgG complexes (c), the human IgG modified tip scanned across the rat anti-human IgG monolayer (d), and the antigen-antibody complexes modified tip scanned across rat anti-human IgG monolayer (e) recorded by CM-AFM, respectively. The CM-AFM was operated in PBS buffer solution with typical scanning rate of 2 Hz and scanning size of 2 μm × 2 μm.

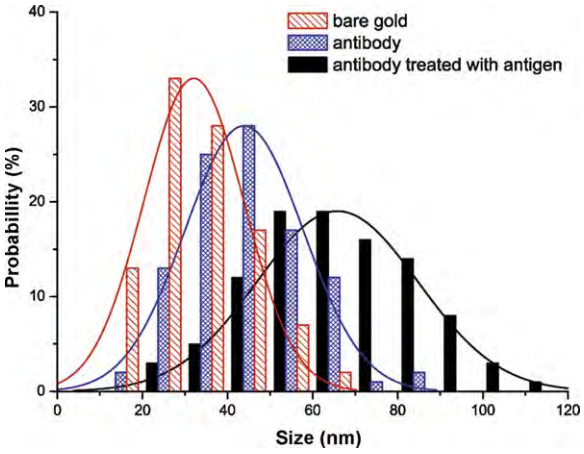

Fig. 4. Size (diameter) distribution histogram of the bare gold, the antibody monolayer and further treated with free antigen were represented by red, blue, and black bars, respectively. Typically, the particles of the bare gold, the antibody monolayer and the antibody treated with antigen have diameters of 20–40 nm, 30–50 nm and 50–90 nm, respectively. The solid lines are theoretical Gaussian distribution curves. (For interpretation of the references to color in this figure legend, the reader is referred to the web version of the article.)

2.5. Tip functionalization

Protocol of tip functionalization is analogous to that of protein immobilization. First, the tip was cleaned in piranha solution for 30 min and washed with ultra pure water, then modified with 1 mM MHA through SAM method. The MHA-modified tips were activated by EDC and NHS in PBS buffer solution to form active esters, then subject to incubation in 10 μg/mL human IgG PBS solution at 4 °C for 6 h. Finally, the specimens were stored in PBS solution at 4 °C. Notably, if not specified, the tips used in this study were bare tips without modification.

2.6. AFM imaging

All images were acquired using Benyuan CSPM 5000 scanning probe microscope (Benyuan Co., China) equipped with a 26-μm E scanner. Commercial Si_3N_4 cantilevers with gold coated on both sides were chosen. The cantilevers with triangular shape and with nominal spring constant of 0.07 N/m (BudgetSensors) were used in CM-AFM. For TM-AFM, the AFM tips with resonance frequency about 70 kHz (Olympus) were employed. All AFM images were operated in PBS buffer solution with typical scanning rate of 2.0 Hz and scanning size of 2 μm × 2 μm. A number of imaging cycles were conducted for CM-AFM and TM-AFM.

The bare gold, the antibody monolayer, and further treated with free antigen, were imaged by CM-AFM and TM-AFM. The sizes of these three different particles were analyzed by CSPM Image 4.62 software program (provided by the manufacturer). Another kind of recognition profile was obtained by performing the antigen modified AFM tip scanned over the antibody monolayer in CM-AFM. For TM-AFM, both topographic and phase images were simultaneously recorded by simply clicking the option of "phase imaging".

2.7. Control experiment for CM-AFM

Blocking experiment was conducted to confirm the specific interaction between antigen and antibody, which was done as follows: firstly, the antigen-fixed tips were incubated for 30 min in the antibody solution to block the binding sites of antigen. Then, the topographic images of antibody monolayer scanned by the antigen-antibody complexes modified AFM tip were performed in the conditions as in Section 2.6.

2.8. Materials

16-Mercaptohexadecanoic acid (MHA), 1-ethyl-3-(dimethylaminopropyl) carbodiimide hydrochloride (EDC), and N-hydroxysulfosuccinimide (NHS) were purchased from Sigma–Aldrich Chemical Co. and used as received. Phosphate buffered saline (PBS, 140 mM NaCl, 3 mM KCl, pH 7.4) and ethanol (guaranteed grade) were purchased from Merck Co., and ultra pure water (resistivity of 18.2 MΩ cm) was obtained by Millipore purification system. Human IgG and rat anti-human IgG were purchased from Biosun Co. (China).

3. Results and discussion

3.1. Preparation of protein monolayers

Since the sensitivity and reproducibility of bioassays are influenced by the surface properties, protein immobilization needs to be carefully considered. The SAM method is reliable for protein immobilization because it ensures the activity, mobility and stability of protein molecules [18,26]. Firstly, it is known that 1 mM thiol and immersion time for 24 h are often sufficient for forming well-ordered thiol film [21]. Secondly, MHA with long carbon chain acted as a spacer to minimize the interference between protein molecules and gold substrate [27]. Thirdly, immobilization conditions were controlled at 4 °C and under PBS buffer solution thoroughly. Moreover, mimicking the natural status of protein molecules requires that the modified protein monolayer should not just provide optimal orientation but also with minimal steric hindrance. Our previous experiments demonstrated the SAM method is reproducible and the formed protein monolayer is well ordered [28].

3.2. Topographic images in CM-AFM demonstrate binding events between antigen and antibody

A topographic image of the bare gold was recorded in PBS buffer solution using a bare AFM tip as a comparison (Fig. 3a). The periodic flat island-like structures were observed, suggesting good uniformity for gold substrates. The antibody (rat anti-human IgG) molecules were covalently immobilized on thiols modified gold substrates by SAM method that yielded a high surface coverage. The topography of the obtained protein monolayer was imaged by CM-AFM (Fig. 3b). The surface shows a number of homogeneous sphere-like structures, which was expected from a densely packed protein monolayer [29]. IgG (~150 kDa) consists of three fragments, two separate and identical Fab fragments with active sites for antigen binding and one Fc fragment. The three dimensional structure is either T- or Y-shaped with a size of 14.2 nm × 8.5 nm × 3.8 nm, as revealed by X-ray diffraction [30] and acknowledged as large biological molecule. The observed single sphere-like structure has larger size than that of a single protein molecule, a fact due to the tip broaden effect and the densely package of protein molecules. The antibody monolayer was incubated with antigen for yielding antigen–antibody complexes, and sequentially subject to CM-AFM imaging. Compared to the surface of the antibody monolayer, the surface of the antigen–antibody complexes shows distinct structures with different shapes and much larger size of the image profile (Fig. 3c), suggesting specific interaction of antigen–antibody and effect of antigen–antibody complexes formation [31–33].

Imaging with the antigen (human IgG) fixed AFM tip in conditions identical to previously used to scan across the protein monolayer resulted in unique images (Fig. 3d). These recognition profiles arose from the binding of antigen on the AFM tip to antibody molecules on the substrate, which led to a deformation of

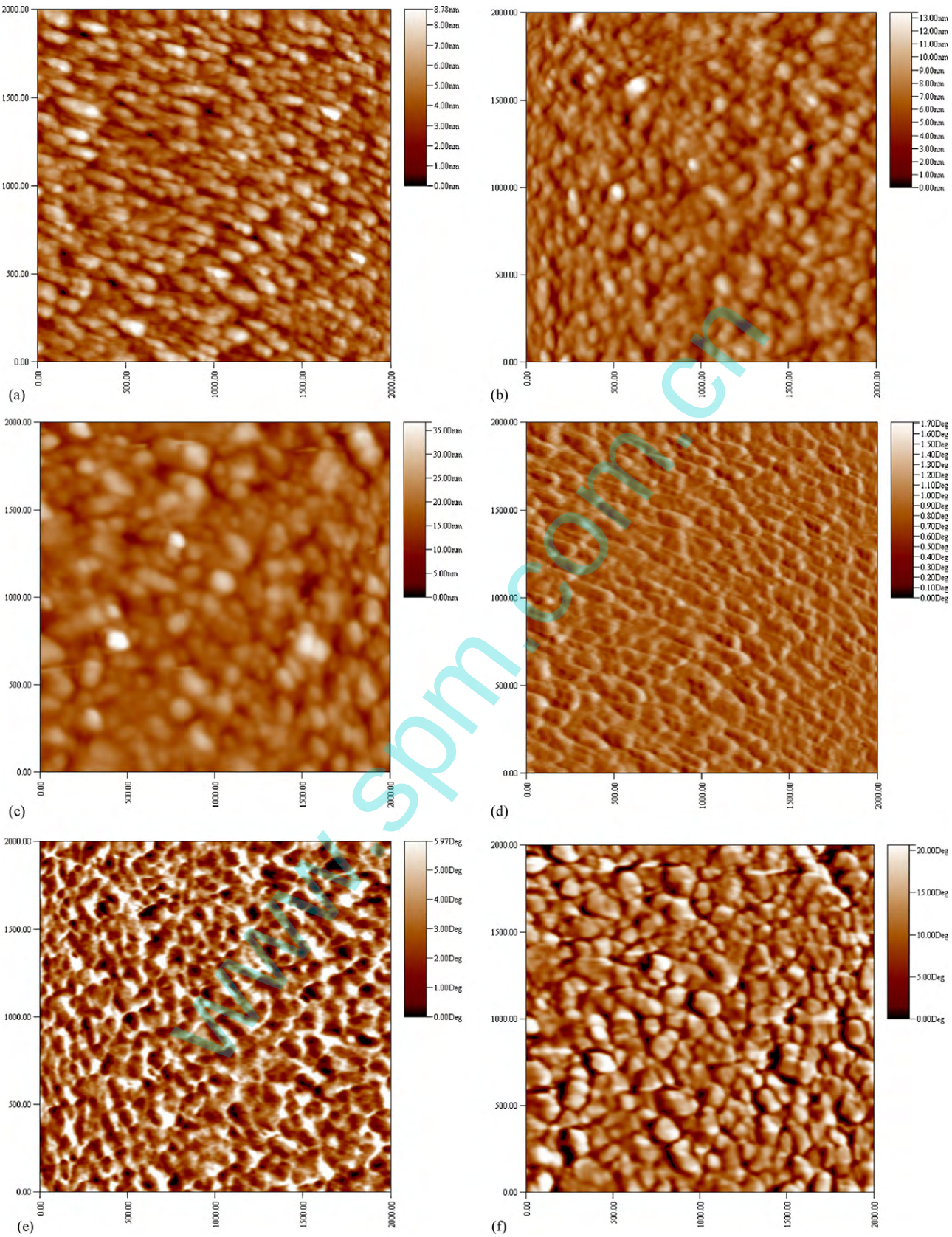

Fig. 5. Topographic images of the bare gold (a), the rat anti-human IgG monolayer (b), the human IgG/rat anti-human IgG complexes (c) and their corresponding phase image (d, e and f, respectively). The CM-AFM was operated in PBS buffer solution with typical scanning rate of 2 Hz and scanning size of 2 μm × 2 μm.

the antibody monolayer. The specificity of the recognition profiles was testified by an antibody blocking experiment. The AFM tip was incubated with free antibody solution led to the disappearance of the recognition profiles (Fig. 3e). This can be explained by free antibody binding to the active binding sites of the antigen molecules, thereby blocking recognition events between antigen and antibody. The antibody monolayer scanned with such modified AFM tip shows plateau-like structures (Fig. 3e). A reasonable explanation is the antigen–antibody complexes modified AFM tip has a large tip radius, tip broaden effect would be heavily introduced when the tip scans across the surface, finally obscures its "real" topography.

For obtaining high quality images in CM-AFM, some aspects require to be noticed: (1) biological materials are usually soft, and the force applied to the cantilever is often lower than 100 pN, otherwise the AFM stylus will deform the biological sample to some extent; (2) when imaging in buffer solution, the long range electrostatic double-layer forces (several tens of nm) are governed by the charge density of both interacting surfaces, the pH and the electrolyte composition of the buffer solution. As a result, the electrostatic forces can be regulated by adjusting the pH and the ionic strength of the buffer solution [34]. In present study, a PBS buffer solution was adopted for simulating the physiological environment; (3) adjusting the instrumental parameters, such as "set point" and "gain", is essential to acquire high quality images. Or else image artifacts will occur, such as tilt of the surface or deformation of sample [17]; (4) the AFM tip is prone to contamination, especially at nano-scale. One should carefully address this issue for each experimental step.

3.3. Size analysis of the observed nanostructures on CM-AFM images

The size (diameter) of the nanostructures observed on the images of the bare gold, the antibody monolayer with or without antigen treatment was analyzed, respectively. Fig. 4 shows the histogram of the size distribution of the structures associated with the three different materials. The mean size of the observed surface structure on the bare gold substrate, which may serve as a reference, was found to be 31.65 (20–40) nm (Fig. 4, red bar). After deposition of antibody molecules onto the bare gold, the mean size of the observed surface structures increased 43.97 (30–50) nm (Fig. 4, blue bar). Considering the tip broaden effect according to Eq. (3) for a tip of $R = 25$ nm (data given by the tip manufacturer), this observed size is very close to the theoretical estimation of projected size, 40.26 nm, for the IgG molecule of real size at 14.2 nm [30], strongly suggesting that the observed structures are indeed the antibody molecules immobilized onto the gold substrate. After treated with free antigen, however, the mean size of surface structures on the antibody monolayer significantly increased to 67.5 (50–90) nm (Fig. 4, black bar). This observed size corresponds to a structure of real size at 34 nm that is more than double of the size of antibody molecule itself, indicating that antigen bound to antibody and formed antibody–antigen complexes.

3.4. Topographical and phase images in TM-AFM reveal recognition events between antigen and antibody

One of the advantages of TM-AFM is a significant reduction of the lateral dragging force allowing more reproducible results to be obtained. This is favorable for imaging biological samples. However, the resolution with TM-AFM is not superior to that of CM-AFM because the compression with the tapping is actually larger than the minimum applied force exerted by the cantilever [35]. Topographic images of the bare gold, the antibody monolayer and the antibody monolayer treated with free antigen solution are shown in Fig. 5a, b and c, respectively. Typically, the surfaces of the bare gold, the antibody monolayer and the antigen–antibody complexes display island-like structures (Fig. 5a), small spherical structures (Fig. 5b) and large spherical (about double size of observed antibody molecule) structures (Fig. 5c), respectively. These results are consistent with the CM-AFM topographic images. The observed discrepancies among three different surfaces indicate that the protein molecules were adequately bound onto the gold substrate, and complexes were successfully formed because of the existence of specific interactions between antigen and antibody. In addition to topographic images, the phase images were simultaneously recorded to verify and explain the surface properties. With respect to the phase images of the bare gold (Fig. 5d), the antibody monolayer (Fig. 5e), and the antigen–antibody complexes (Fig. 5f), the greater phase lag of the tip's driven frequency, the brighter pixels appear in the phase image [20]. All phase images show patch-like surfaces but distinct nanostructures. The phase images are likely to serve as the clearer 'topographical images' and are often adopted to observe fine surface nanostructures that cannot be visualized in the topographic images [36]. Present study confirmed that phase images not only highlight edges but also give clearer phase contrast. Thus, it is convincing that phase images can serve beyond topographies.

Usually, two classes of factors may be responsible for the phase shift of the oscillating cantilever. One is of instrumental parameters, such as the amplitude modulation feedback, the driving frequency, the tip's sharpness and the spring constant [37–39]. The other is of chemical or physical properties of the material surfaces, including viscoelasticity, friction, adhesion and components [40–42]. To date, several theoretical models have been proposed to explain phase behavior [37,43,44]. For example, Magonov and co-workers defined the phase (angle) shift, $\Delta\varphi$, between the free and interacting cantilevers as [40]:

$$\Delta\varphi = \frac{\pi}{2} - \tan^{-1}\left(\frac{k}{Q\sigma}\right) \approx \frac{Q\sigma}{k} \quad (\sigma \le k) \tag{4}$$

where Q is the quality factor, k is the spring constant of a freely oscillating cantilever, and σ is the overall force derivatives. For TM-AFM, the force derivative σ is proportional to time-averaged contact area A, determined by surface stiffness and morphological structure. A softer material leads to a larger contact area A [35]. It is known that flexible protein molecules are soft biomaterials, whereas the gold substrates are stiff. According to Eq. (4), the phase shift of the antibody monolayer is larger than that of the bare gold substrates (1.71°). Since the large contact area of the antigen–antibody complexes, the larger phase shift of the antigen–antibody complexes (20.58°) was observed than that of the antibody monolayer (5.97°). Our experimental results are consistent with these theoretical predictions.

4. Conclusions

We herein present a study of recognition events between antigen and antibody molecules immobilized on SAM modified substrate and visualized by CM-AFM and TM-AFM. Both topographic images by CM-AFM and TM-AFM, and phase images by TM-AFM were obtained. The topographic images of either the bare gold substrate, the rat anti-human IgG monolayer, or the human IgG/rat anti-human IgG complexes show significantly different surface structures, suggesting recognition events occurred between antibody and antigen. This is further supported by phase images with the phase angular variations, which are complementary to topographic images. Moreover, phase imaging can be served as a real time contrast enhancement technique to TM-AFM in terms of highlighting edges and clear observation of fine features. Size analysis of the observed surface structures of different surface compositions demonstrated that the mean size of the observed

structures on the antibody monolayers was very close to what is estimated for the actual size of the antibody molecule. These results, therefore, suggest that providing the sample is prepared appropriately and the instrumental parameters are set adequately, CM-AFM and TM-AFM are capable of detecting recognition events between biological molecules, such as antigen and antibody, and could be useful tools in PPIs studies.

Acknowledgements

This work was supported by the National Natural Science Foundation of China (Nos. 30670496, 30770529) and the Scientific Research Foundation for the Returned Overseas Chinese Scholars, State Education Ministry (2006-331) and the Natural Science Foundation Project of CQ CSTC (2006BB5017).

References

[1] F. Cecchet, A.S. Duwez, S. Gabriel, C. Jerome, R. Jerome, K. Glinel, S. Demoustier-Champagne, A.M. Jonas, B. Nysten, Anal. Chem. 79 (2007) 6488–6495.
[2] W. Lee, B.K. Oh, Y. Min Bae, S.H. Paek, W. Hong Lee, J.W. Choi, Biosens. Bioelectron. 19 (2002) 185–192.
[3] L. Li, S. Chen, S. Oh, S. Jiang, Anal. Chem. 74 (2002) 6017–6022.
[4] P. Hinterdorfer, Y.F. Dufrene, Nat. Methods 3 (2006) 347–355.
[5] H. Zhu, M. Bilgin, M. Snyder, Annu. Rev. Biochem. 72 (2003) 783–812.
[6] W. Kusnezow, A. Jacob, A. Walijew, F. Diehl, J.D. Hoheisel, Proteomics 3 (2003) 254–264.
[7] T.S. Tsapikouni, Y.F. Missirlis, Mater. Sci. Eng. B 152 (2008) 2–7.
[8] R. Karisson, J. Mol. Recognit. 17 (2004) 151–161.
[9] R. Pio, A. Martinez, E.J. Unsworth, J.A. Kowalak, J.A. Bengoechea, P.F. Zipfei, T.H. Elsasser, F. Cuttitta, J. Biol. Chem. 276 (2001) 12292–12300.
[10] A. Roda, P. Pasini, M. Mirasoli, E. Michelini, M. Guardigli, Trends Biotechnol. 22 (2004) 295–303.
[11] N.C. Santos, M.A.R.B. Castanho, Biophys. Chem. 107 (2004) 133–149.
[12] D. Fotiadis, S. Scheuring, S.A. Muller, A. Engel, D.J. Muller, Micron 33 (2002) 385–397.
[13] G.U. Lee, D.A. Kidwell, R.J. Colton, Langmuir 10 (1994) 354–357.
[14] C.D. Frisbie, L.F. Rosznyai, A. Noy, M.S. Wrighton, C.M. Lieber, Science 265 (1994) 2071–2074.
[15] J.P. Cleveland, B. Anczykowski, A.E. Schmid, V.B. Elings, Appl. Phys. Lett. 72 (1998) 2613–2615.
[16] P. Parot, Y.F. Dufrene, P. Hinterdorfer, C. Le Grimellec, D. Navajas, J.L. Pellequer, S. Scheuring, J. Mol. Recognit. 20 (2007) 418–431.
[17] A. Alessandrini, P. Facci, Meas. Sci. Technol. 16 (2005) R65–R92.
[18] L. Guo, R. Wang, H. Xu, J. Liang, Physica. E: Low. Dimens. Syst. Nanostruct. 27 (2005) 240–244.
[19] G.K. Pang, K.Z. Baba-Kishi, A. Patel, Ultramicroscopy 81 (2000) 35–40.
[20] M. Stark, C. Moller, D.J. Muller, R. Guckenberger, Biophys. J. 80 (2001) 3009–3018.
[21] S. Ferretti, S. Paynter, D.A. Russell, K.E. Sapsford, D.J. Richardson, Trends Analyt. Chem. 19 (2000) 530–540.
[22] J.C. Love, L.A. Estroff, J.K. Kriebel, R.G. Nuzzo, G.M. Whitesides, Chem. Rev. 105 (2005) 1103–1169.
[23] C. Stroh, H. Wang, R. Bash, B. Ashcroft, J. Nelson, H. Gruber, D. Lohr, S.M. Lindsay, P. Hinterdorfer, Proc. Natl. Acad. Sci. U.S.A. 101 (2004) 12503–12507.
[24] W.D. Marcus, H. Wang, S.M. Lindsay, M.R. Sierks, Nanomedicine 4 (2008) 1–7.
[25] Z.J. Lv, J.H. Wang, G.P. Chen, L.H. Deng, Nanoscale Res. Lett. 5 (2010) 1032–1038.
[26] M. Lekka, A.J. Kulik, S. Jeney, J. Raczkowska, J. Lekki, A. Budkowski, L. Forro, J. Chem. Phys. 123 (2005) 014702.
[27] D.K. Schwartz, Annu. Rev. Phys. Chem. 52 (2001) 107–137.
[28] Z.J. Lv, J.H. Wang, L.H. Deng, G.P. Chen, Nanoscale Res. Lett. 4 (2009) 1403–1408.
[29] A. Raab, W. Han, D. Badt, S.J. Smith-Gill, S.M. Lindsay, H. Schindler, P. Hinterdorfer, Nat. Biotechnol. 17 (1999) 901–905.
[30] E.W. Silverton, M.A. Navia, D.R. Davies, Proc. Natl. Acad. Sci. U.S.A. 74 (1977) 5140–5144.
[31] M.E. Browning-Kelley, K. Wadu-Mesthrige, V. Hari, G.Y. Liu, Langmuir 13 (1997) 343–350.
[32] P. Hammarstrom, M. Person, U. Carlsson, J. Biol. Chem. 276 (2001) 21765–21775.
[33] C.S. Neish, I.L. Martin, R.M. Henderson, J.M. Edwardson, Br. J. Pharmacol. 135 (2002) 1943–1950.
[34] S. Scheuring, S. Fotiadis, C. Moller, S.A. Muller, A. Engel, D.J. Muller, Single Mol. 2 (2001) 59–67.
[35] J. Yang, Cell Biochem. Biophys. 41 (2004) 435–449.
[36] F. Kienberger, L.T. Costa, R. Zhu, G. Kada, M. Reithmayer, L. Chtcheglova, C. Rankl, A.B. Pacheco, S. Thalhammer, V. Pastushenko, W.M. Heckl, D. Blaas, P. Hinterdorfer, Biomaterials 28 (2007) 2403–2411.
[37] R. Garcia, R. Perez, Surf. Sci. Rep. 47 (2002) 197–301.
[38] X. Chen, M.C. Davies, C.J. Roberts, S.B. Tendler, P.M. Williams, N.A. Burnham, Surf. Sci. 460 (2000) 292–300.
[39] F.J. Giessibl, H. Bielefeldt, Phys. Rev. B: Condens. Matter Mater. Phys. 61 (2000) 9968–9971.
[40] P.J. De Pablo, J. Colchero, M. Luna, J. Gomez-Herrero, A.M. Baro, Phys. Rev. B: Condens. Matter Mater. Phys. 61 (2000) 14179–14183.
[41] R. Hillenbrand, M. Stark, R. Guckenberger, Appl. Phys. Lett. 76 (2000) 3478–3480.
[42] Z. Ye, X. Zhao, J. Microsc. 238 (2010) 27–35.
[43] S.N. Magonov, V. Elings, M.H. Whangbo, Surf. Sci. 375 (1997) L385–L391.
[44] A. Berquand, P.E. Mazeran, J.M. Laval, Surf. Sci. 523 (2003) 125–130.